

AD-F 300 089

12

AD

AD A120046


TECHNICAL REPORT ARBRL-TR-02423

TWC-DIMENSIONAL MODEL FOR ARC DYNAMICS
IN THE RAIL GUN

John D. Powell

October 1982

DTIC
ELECTE
S OCT 6 1982 D
B



US ARMY ARMAMENT RESEARCH AND DEVELOPMENT COMMAND
BALLISTIC RESEARCH LABORATORY
ABERDEEN PROVING GROUND, MARYLAND

Approved for public release; distribution unlimited.

DTIC FILE COPY

82 10 01 002

UNCLASSIFIED

SECURITY CLASSIFICATION OF THIS PAGE (When Data Entered)

REPORT DOCUMENTATION PAGE		READ INSTRUCTIONS BEFORE COMPLETING FORM
1. REPORT NUMBER Technical Report ARBRL-TR-02423	2. GOVT ACCESSION NO. AD-A120046	3. RECIPIENT'S CATALOG NUMBER
4. TITLE (and Subtitle) TWO-DIMENSIONAL MODEL FOR ARC DYNAMICS IN THE RAIL GUN		5. TYPE OF REPORT & PERIOD COVERED
		6. PERFORMING ORG. REPORT NUMBER
7. AUTHOR(s) John D. Powell		8. CONTRACT OR GRANT NUMBER(s)
9. PERFORMING ORGANIZATION NAME AND ADDRESS US Army Ballistic Research Laboratory ATTN: DRDAR-BLB Aberdeen Proving Ground, MD 21005		10. PROGRAM ELEMENT, PROJECT, TASK AREA & WORK UNIT NUMBERS RDT&E 1L161102AH43
11. CONTROLLING OFFICE NAME AND ADDRESS US Army Armament Research & Development Command US Army Ballistic Research Laboratory (DRDAR-BL) Aberdeen Proving Ground, MD 21005		12. REPORT DATE October 1982
		13. NUMBER OF PAGES 49
14. MONITORING AGENCY NAME & ADDRESS (if different from Controlling Office)		15. SECURITY CLASS. (of this report) UNCLASSIFIED
		15a. DECLASSIFICATION/DOWNGRADING SCHEDULE
16. DISTRIBUTION STATEMENT (of this Report) Approved for public release; distribution unlimited.		
17. DISTRIBUTION STATEMENT (of the abstract entered in Block 20, if different from Report)		
18. SUPPLEMENTARY NOTES		
19. KEY WORDS (Continue on reverse side if necessary and identify by block number) Electric gun, rail gun, electromagnetic propulsion, plasma dynamics, fluid mechanics		
20. ABSTRACT (Continue on reverse side if necessary and identify by block number) (idx) A two-dimensional model is suggested for describing the fluid-mechanical, elec- trodynamic properties of the plasma in an arc-driven rail gun. The analysis includes deriving a set of general, time-dependent equations, the solution of which yields the associated properties of the arc. These equations are then solved under the assumptions that the flow variables are steady in a frame of reference which accelerates with the arc, and that the effect of the arc's acceleration upon these variables can be neglected. (Continued)		

DD FORM 1 JAN 73 1473

EDITION OF 1 NOV 65 IS OBSOLETE

UNCLASSIFIED

SECURITY CLASSIFICATION OF THIS PAGE (When Data Entered)

UNCLASSIFIED

SECURITY CLASSIFICATION OF THIS PAGE(When Data Entered)

Numerical calculations are carried out to analyze arcs in both recent and proposed experiments. In addition to the numerical calculations, some approximate analytic solutions, which are applicable under certain limiting conditions, are also worked out. These limiting-case solutions are then used to derive a set of scaling relations which indicate how the arc properties vary with gun size, projectile mass, and acceleration characteristics. Considerable discussion of the assumptions and the results is given, emphasizing particularly the physical reasons for the differences with previous one-dimensional calculations.

UNCLASSIFIED

SECURITY CLASSIFICATION OF THIS PAGE(When Data Entered)

TABLE OF CONTENTS		Page
LIST OF FIGURES		5
LIST OF TABLES		7
I.	INTRODUCTION	9
II.	MATHEMATICAL FORMALISM	12
III.	SOLUTION OF EQUATIONS	18
	A. General Remarks and Additional Approximations	18
	B. Limiting-Case Analytic Solution	20
	1. Case I	22
	2. Case II	23
	3. Comparison of Two Solutions	23
	C. Numerical Technique	24
	D. Analysis of Rashleigh-Marshall Experiment	25
	E. Analysis of Westinghouse Experiment	33
	F. Scaling Relations and Optimum Arc Materials	35
IV.	DISCUSSION	39
ACKNOWLEDGEMENT.		43
REFERENCES.		45
DISTRIBUTION LIST		47



3/4

Accession For	
NTIS GRA&I	<input checked="checked" type="checkbox"/>
DTIC TAB	<input type="checkbox"/>
Unannounced	<input type="checkbox"/>
Justification	
By	
Distribution/	
Availability Codes	
Dist	Avail and/or Special
A	

LIST OF FIGURES

<u>Figure</u>		<u>Page</u>
1.	Model for Arc Calculations	11
2.	Pressure, in Pascals, as a Function of ξ	28
3.	Magnetic Induction Field, in Tesla, as a Function of ξ	29
4.	Lines of Constant Temperature, in Degrees Kelvin, Within the Arc	30
5.	Lines of Constant Mass Density, in kg/m^3 , Within the Arc	31
6.	Lines of Constant Electron Density, in m^{-3} , Within the Arc . . .	32

LIST OF TABLES

<u>Table</u>		<u>Page</u>
I	Experimental Data for Rashleigh-Marshall Experiment	26
II	Results of Numerical Calculations for Rashleigh-Marshall Experiment	27
III	Experimental Data for Westinghouse Gun	34
IV	Results of Numerical Solution for Westinghouse Gun	34
V	General Scaling Factors	36
VI	Scaling Factors as a Function of Arc Length	37
VII	Comparison of Numerical and Scaling-Relation Results for Westinghouse Experiment	38

I. INTRODUCTION

In some recent work,¹ we exposed a one-dimensional model and developed a formalism for studying plasma dynamics in an arc-driven rail gun. A set of governing equations was derived and solved numerically to determine the properties of the arc for various rail guns, projectile masses, and accelerating characteristics. Approximate analytic solutions to the resulting equations were also obtained and, from these solutions, some scaling relations were derived. The extent to which the resulting solutions accurately represent the arc's characteristics was assessed, and the necessity for extending the work to two dimensions was emphasized. In this report that extension is undertaken.

The rationale for the Army's interest in rail guns was thoroughly discussed in Ref. 1 and will not be discussed here. It is well to point out, however, that the most successful rail-gun experiments undertaken thus far have employed a plasma arc to drive the projectile. No doubt the success of these experiments results from the ability of the arc to maintain better contact with the rails than can the sliding contacts used in solid-armature rail guns. At the higher velocities anticipated in future experiments an arc armature is likely to be indispensable. Consequently, it is important to assess the properties of the arc, to determine its erosive effects on the rails and projectile, and indeed to determine the feasibility of using arcs in rail guns sufficiently large to be of military interest.

Before turning to the calculations in this report we will summarize some of the more recent developments in rail-gun technology. Westinghouse, under DARPA/ARRADCOM support, has nearly completed construction of a large gun intended to accelerate a 300-g projectile to 3 km/s in about 3 m. The current intention in that experiment is to use a solid armature in the initial stages but, after transfer of the gun to Dover, some experiments employing an arc are intended. Arc-driven rail-gun experiments² have been undertaken most recently by a team from Los Alamos and Livermore. They have constructed rail guns which use a magnetic-flux compression generator as a primary power supply, and have successfully accelerated projectiles of a few grams to several kilometers per second. In addition, in one experiment, a 165-g projectile was accelerated to about 350 m/s. The latter effort represents the most massive projectile yet accelerated by a rail gun. In addition to these experiments, BRL has recently initiated an experimental program and has constructed a small rail gun powered by a capacitor bank. The intention of the present and near-future experiments at BRL will be to analyze the properties of the arc in some detail, rather than to accelerate ever-more-massive projectiles to ever-higher velocities.

1. John D. Powell and Jad H. Batteh, "Plasma Dynamics of the Arc-Driven Rail Gun," Ballistic Research Laboratory Report No. ARBRL-TR-02267, September 1980. See also "Plasma Dynamics of an Arc-Driven, Electromagnetic, Projectile Accelerator," *J. Appl. Phys.* **52**, 2717 (1981). (AD A092345)
2. R.S. Hawke, A.L. Brooks, F.J. Deadrick, J.K. Scudder, C.M. Fowler, R.S. Caird, and D.R. Peterson, "Results of Rail Gun Experiments Powered by Magnetic Flux Compression Generators," *IEEE Trans. Magnetics* **18**, 821 (1982).

Some diagnostic measurements have been undertaken already, and more sophisticated ones are planned for the immediate future.

In the present calculation we wish to employ the same model and assumptions that were used in Ref. 1. A schematic diagram of the model is shown in Fig. 1. Sides one and two represent the rails, which are infinitely extended in the z direction, and which carry current in the direction indicated. Side three represents the power supply and side four contains both the arc (between $x = x_0$ and $x = \ell$) and the projectile (shaded area). The resulting current configuration produces a magnetic field in the space between the rails, and this field interacts with the current through the arc, accelerating both it and the projectile in the x direction.

The intention of the calculation is to determine the fluid-dynamical properties of the arc, the electromagnetic fields associated with it, and the acceleration imparted to the arc and projectile. In Ref. 1, these properties were assumed to vary only in the direction of acceleration, while in the present work variations in one transverse direction, the y direction, will also be allowed. The additional assumptions employed and justified in Ref. 1 will also apply to this calculation: First, since the conductivity of the rails is several orders of magnitude higher than that of the arc, we simplify the problem by assuming that the rails are actually perfect conductors. The finite conductivity of the arc, however, is accounted for. Second, we assume that the plasma is at most doubly ionized and neglect higher degrees of ionization. This assumption, while not fundamental to the calculation, greatly simplifies the algebra and is probably not unreasonable in the temperature ranges under consideration. Third, we assume that energy losses within the arc occur only by radiation and neglect ordinary heat conduction. As was demonstrated explicitly in Ref. 1, heat conduction is negligible at the temperatures which characterize arcs in rail guns of experimental interest. Fourth, we assume that the current per unit height on the surface of the rails is constant in time. This condition can be satisfied in practice by using as a power source an inductive store having a sufficiently high inductance. We will also assume in the present treatment that the gas is inviscid.

In addition to the above assumptions, we also assumed in the one-dimensional calculations that the properties of the arc were steady in a frame of reference that accelerated with the projectile, and demonstrated that the governing equations possessed a solution in that limit. In the two-dimensional case, as we shall see, no such solution exists for the steady situation in which the arc is at rest relative to the projectile. However, if the effect of the arc's acceleration upon its fluid-dynamical properties can be neglected, then a steady solution similar to the one-dimensional case does exist. We shall assume this to be the case in our actual numerical calculations, although we will derive a time-dependent formalism in order to make possible more general calculations in the future. The physical reasons for the differences between the one- and two-dimensional cases are discussed in Sec. III of the report, and some discussion of the significance of neglecting the acceleration is given in Sec. IV.

Before discussing the present work, it is necessary to indicate the rationale for undertaking a two-dimensional calculation and what differences

might be expected with regard to the one-dimensional results. In Ref. 1 it was demonstrated that of all the energy deposited into the model rail-gun system by the power supply, slightly less than half of the energy became associated with kinetic energy of the arc and projectile. An equal amount was stored in the magnetic field and the remaining energy, a small fraction of the total, was dissipated in the arc. In a two-dimensional calculation a similar conclusion should hold and, since energy must still be conserved, the projectile will have essentially the same kinetic energy and an equivalent amount of energy should be stored in the field. Consequently, the arc pressure, which accelerates the projectile, will have to be similar. On the other hand, it is evident that more surface area is available for radiation in the two-dimensional calculation, so the temperature of the arc should be significantly smaller. Similarly, the mass density will be larger in the two-

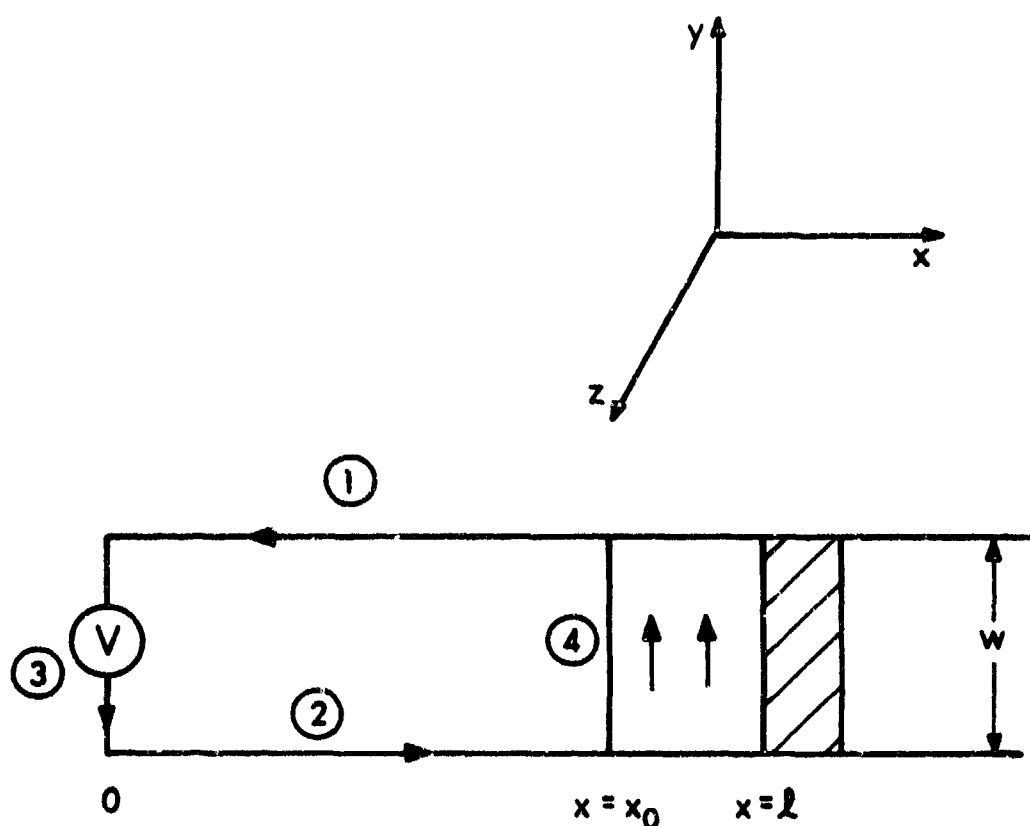


Figure 1. Model for Arc Calculations

dimensional case, since it must increase as the temperature decreases to satisfy the equation of state (assuming constant pressure and degree of ionization). It is clear, therefore, that a one-dimensional model probably overestimates the temperature in the arc, underestimates the density, and gives fairly accurate results for the pressure and fields. However, a two-dimensional model not only allows for radiation at the front and the back of the arc, but also along the surfaces in contact with the rails. Since these latter surfaces are usually large in experiments of interest, a significant improvement in the temperature and density calculations should be anticipated.

In addition, it was found that the one-dimensional calculation predicted a rather anomalous, nonphysical manner in which the temperature varied with the length of the arc. Intuitively, one expects that as the length increases the temperature should fall, since the resistance of the arc becomes smaller. However, it was shown in Ref. 1 that the temperature remained essentially constant as the arc length was increased. The reason for this unexpected behavior was that, as the length increased, the temperature gradients within the arc also became smaller. Consequently, the energy dissipated was radiated away less efficiently. In the one-dimensional problem the two effects (smaller dissipation and less efficient radiation) almost exactly compensated each other with the result that little variation in the temperature was observed. As was pointed out, however, this unusual effect was just a peculiarity of the one-dimensional model and, for a two- or three-dimensional case, the temperature should be expected to fall with increasing arc size. The present calculation, therefore, should predict in some detail how that variation occurs.

The organization of the report is the following. In Sec. II the time-dependent formalism for treating the two-dimensional problem is developed and the appropriate set of governing equations derived. In Sec. III, the approximations employed in the solution of the equations are discussed, and numerical as well as approximate analytic solutions to the equations are obtained for several cases of interest. In addition, a set of approximate scaling relations is derived which indicate how arc properties vary with gun size, projectile mass, and acceleration characteristics. Finally, in Sec. IV, some discussion of the results is given.

II. MATHEMATICAL FORMALISM

In this section we will be concerned with deriving the equations which determine the electromagnetic fields associated with the arc, its fluid-dynamical characteristics, and the acceleration of the arc and projectile. A general, time-dependent formalism will be worked out here, though additional approximations will be made in the following section where the solution is carried out.

Applying Maxwell's equations in the space between $x = x_0$ and $x = \ell$ in Fig. 1, we have

$$\vec{\nabla} \times \vec{B} = \mu \vec{J} \quad (2.1)$$

$$\vec{\nabla} \times \vec{E} = - \frac{\partial \vec{B}}{\partial t} \quad (2.2)$$

and

$$\vec{J} = \sigma (\vec{E} + \vec{v} \times \vec{B}) \quad (2.3)$$

In these equations \vec{B} represents the magnetic-induction field, \vec{E} the electric-field intensity, \vec{J} the current density, \vec{v} the plasma material velocity, σ the plasma conductivity, and μ the permeability which is assumed to be that of free space. The displacement current has been neglected in Eqs. (2.1)-(2.3), since the propagation velocities under consideration are small compared to the speed of light.

It is convenient to make a transformation to a dimensionless coordinate system which accelerates with the arc. Specifically, we let

$$\xi = \frac{x-x_0}{l_a} \quad \eta = y/w \quad (2.4)$$

where $l_a = l - x_0$ is the distance from the projectile to the trailing edge of the arc. The transformation is then effected by noting that

$$\begin{aligned} \frac{\partial}{\partial x} &= \frac{1}{l_a} \frac{\partial}{\partial \xi} & \frac{\partial}{\partial y} &= \frac{1}{w} \frac{\partial}{\partial \eta} \\ \frac{\partial}{\partial t} &= \frac{\partial}{\partial t'} - \frac{v_0}{l_a} \frac{\partial}{\partial \xi} - \frac{\xi}{l_a} \frac{\partial l_a}{\partial t'} \frac{\partial}{\partial \xi} \end{aligned} \quad (2.5)$$

where v_0 is the velocity of the trailing edge of the arc and where the notation $\partial/\partial t'$ is used to denote the time derivative measured in the moving frame.

We now take the curl of Eq. (2.1), note that $\vec{\nabla} \cdot \vec{B}$ is zero, and use Eq. (2.2) to obtain a differential equation for \vec{B} in terms of the conductivity and plasma velocity. After considerable simplification we find that the appropriate equation in the new coordinate system is

$$\begin{aligned} l_a^2 w^2 \mu \sigma \frac{\partial B}{\partial t'} &= w^2 \frac{\partial^2 B}{\partial \xi^2} + l_a^2 \frac{\partial^2 B}{\partial \eta^2} - w^2 \frac{\partial \log \sigma}{\partial \xi} \frac{\partial B}{\partial \xi} - l_a^2 \frac{\partial \log \sigma}{\partial \eta} \frac{\partial B}{\partial \eta} \\ &- \mu \sigma l_a w \left[w v'_x \frac{\partial B}{\partial \xi} + l_a v'_y \frac{\partial B}{\partial \eta} + w B \frac{\partial v'_x}{\partial \xi} + l_a B \frac{\partial v'_y}{\partial \eta} \right] \\ &+ \mu \sigma l_a w^2 \xi \frac{\partial l_a}{\partial t'} \frac{\partial B}{\partial \xi} \end{aligned} \quad (2.6)$$

In writing Eq. (2.6) we have noted that, from symmetry, \vec{B} has only a single component in the z direction and have defined \vec{v}' as the plasma velocity relative to the trailing edge, i.e.,

$$\vec{v}' = \vec{v} - \vec{v}_0 \quad . \quad * \quad (2.7)$$

Once the induction field has been determined from Eq. (2.6), the current density \vec{J} and electric-field intensity \vec{E} then follow directly from Eqs. (2.1) and (2.3), respectively.

The fluid-dynamic properties of the arc are determined largely from equations which express the conservation of mass, momentum, and energy for the arc as a whole. Specifically, we have

$$\frac{\partial \rho}{\partial t} + \vec{\nabla} \cdot (\rho \vec{v}) = 0 \quad (2.8)$$

$$\rho \frac{\partial \vec{v}}{\partial t} + \rho \vec{v} \cdot \vec{\nabla} \vec{v} + \vec{\nabla} \cdot \vec{P} = \vec{F} \quad (2.9)$$

$$\rho \frac{\partial e}{\partial t} + \rho \vec{v} \cdot \vec{\nabla} e + \vec{\nabla} \cdot \vec{q} + \vec{P} : \vec{\nabla} \vec{v} = J^2 / \sigma \quad (2.10)$$

In these equations ρ represents the plasma density and e its specific internal energy; \vec{P} is the second-order pressure or momentum-flux tensor; \vec{q} is the heat flux which accounts for losses due to radiation and conduction; finally, \vec{F} is the force per unit volume acting on the plasma and, for the problem at hand, it is given by

$$\vec{F} = \vec{J} \times \vec{B} \quad (2.11)$$

As before, it is convenient to transform Eqs. (2.8)-(2.10) to the moving frame. Using Eq. (2.5), we find

$$l_a w \frac{\partial \rho}{\partial t'} = - w v_x' \frac{\partial \rho}{\partial \xi} - l_a v_y' \frac{\partial \rho}{\partial \eta} - w \rho \frac{\partial v_x'}{\partial \xi} - l_a \rho \frac{\partial v_y'}{\partial \eta} + w \xi \frac{\partial l_a}{\partial t'} \frac{\partial \rho}{\partial \xi} \quad (2.12)$$

$$l_a \rho w \frac{\partial v_x'}{\partial t'} = - \rho l_a w \alpha - w \rho v_x' \frac{\partial v_x'}{\partial \xi} - l_a \rho v_y' \frac{\partial v_x'}{\partial \eta} - w \frac{\partial P}{\partial \xi} - \frac{w B}{\mu} \frac{\partial B}{\partial \xi} + \rho \xi w \frac{\partial l_a}{\partial t'} \frac{\partial v_x'}{\partial \xi} \quad (2.13)$$

* Unprimed quantities will be used throughout to refer to quantities measured in the fixed frame and primed variables to those measured in the moving frame. In the nonrelativistic limit we have, for example,

$$\vec{J}' = \vec{J}$$

$$\vec{B}' = \vec{B}$$

$$\vec{E}' = \vec{E} + \vec{v} \times \vec{B} \quad .$$

$$\begin{aligned}
l_a w \rho \frac{\partial v_y'}{\partial t'} = & - w \rho v_x' \frac{\partial v_y'}{\partial \xi} - l_a \rho v_y' \frac{\partial v_y'}{\partial \eta} - l_a \frac{\partial p}{\partial \eta} - \frac{l_a B}{\mu} \frac{\partial B}{\partial \eta} \\
& + \rho \xi w \frac{\partial l_a}{\partial t'} \frac{\partial v_y'}{\partial \xi}
\end{aligned} \quad (2.14)$$

and

$$\begin{aligned}
l_a w \rho \frac{\partial e}{\partial t'} = & - w \rho v_x' \frac{\partial e}{\partial \xi} - l_a \rho v_y' \frac{\partial e}{\partial \eta} - w \frac{\partial q_x}{\partial \xi} - l_a \frac{\partial q_y}{\partial \eta} \\
& - w p \frac{\partial v_x'}{\partial \xi} - l_a p \frac{\partial v_y'}{\partial \eta} + l_a w J^2 / \sigma + \rho w \xi \frac{\partial l_a}{\partial t'} \frac{\partial e}{\partial \xi}.
\end{aligned} \quad (2.15)$$

In obtaining the above results we have replaced p by the hydrostatic pressure P since the gas is inviscid, have used Eqs. (2.1) and (2.11) to express the force \vec{F} solely in terms of the induction field, and have denoted by a the acceleration of the trailing edge of the arc. The resulting equations are identical to those generally encountered in fluid mechanics except for the forces which are electromagnetic in origin and except the term proportional to J^2/σ which accounts for the Joule heating of the plasma. It should also be noted that the term which varies with a is an effective force on the plasma that arises because the reference frame is not inertial; such a force does not arise in the more customary laboratory-frame calculations.

Equations (2.12)-(2.15) are insufficient to determine the flow parameters uniquely and we need, in addition, the internal energy as a function of P and the temperature T , an equation of state relating P to T and ρ , and finally a representation of the heat flux \vec{q} . For simplicity, we assume an ideal-gas equation of state so that

$$P = \frac{(1 + x_1 + 2 x_2) k_B T \rho}{m_0} \quad (2.16)$$

where m_0 is the atomic mass of the ions or neutrals constituting the arc, k_B is Boltzmann's constant, and x_1 and x_2 are the concentrations of singly and doubly ionized atoms, respectively. These concentrations can be determined from the Saha equations which, for a singly and doubly ionized gas, can be written³

3. Y.B. Zel'dovich and Y.P. Raizer, Physics of Shock Waves and High-Temperature Hydrodynamic Phenomena, (Academic, New York, 1966), Vol. I, Chap. 3.

$$\frac{x_1 (x_1 + 2 x_2)}{(1 - x_1 - x_2)(1 + x_1 + 2x_2)} = K_1 (T, P) \quad (2.17)$$

$$\frac{x_2 (x_1 + 2x_2)}{x_1 (1 + x_1 + 2x_2)} = K_2 (T, P) ,$$

where

$$K_{j+1} = \frac{2}{P} \frac{Z_j + 1}{Z_{ij}} \left(\frac{m_e}{2\pi\hbar} \right)^{3/2} (k_B T)^{5/2} e^{-I_{j+1}/k_B T} . \quad (2.18)$$

In Eq. (2.18), m_e is the electron mass, \hbar is Planck's constant divided by 2π , and I_j is the energy needed to ionize the atom j times. The quantity Z_j represents the electronic partition function for the j th ion; specifically, it is given by

$$Z_j = \sum_i g_{ji} e^{-u_{ji}/k_B T} \quad (2.19)$$

where u_{ji} is the energy of the i th electronic state of the j th ion and where g_{ji} is the appropriate degeneracy factor for this level. Values of these parameters for copper and its first two ions have been tabulated elsewhere.^{4,1}

In the temperature range with which we will be concerned, the major source of energy loss within the arc is radiation and ordinary heat conduction can be neglected. Furthermore, if the radiation mean free path is small compared to the dimensions of the arc, as we will find to be the case, the radiation flux can be represented by⁵

$$\vec{q} = - \frac{16 \sigma_S \lambda T^3}{3} \nabla T \quad (2.20)$$

where σ_S is Stefan's constant and λ is the mean free path. Expressions for λ have been worked out and, for the problem at hand, we will use the relation⁶

$$\lambda(\xi, n) = \frac{0.91 \times 10^{11} k_B T^3 (1+x_1+2x_2)}{P[1-x_1-x_2]e^{-I_1/k_B T} + 4x_1 e^{-I_2/k_B T} + 9x_2 e^{-I_3/k_B T}} . \quad (2.21)$$

4. C.E. Moore, "Atomic Energy Levels," National Bureau of Standards Circ. No. 467, Vol. II, Washington, DC, 1952.

5. See Ref. 3, Chap. 2.

6. Y.P. Raizer, "Simple Method for Computing the Mean Range of Radiation in Ionized Gases at High Temperatures," Sov. Phys.-JETP 37, 769 (1960). See also Ref. 3, Chap. 5.

The remaining information needed to complete the system of equations describing the arc properties are expressions for the arc length l_a and the conductivity σ . If we define ρ_{l_a} as the mean plasma density multiplied by its length along the x axis, we have the obvious condition

$$l_a = \frac{\rho_{l_a}}{\int d\xi \int dn \rho(\xi, n)} \quad (2.22)$$

For all cases of interest in the present problem, we will find that the plasma is almost completely ionized with few neutrals being present in the arc. Consequently, the conductivity can be well approximated by that for a completely ionized gas, namely,⁷⁻⁹

$$\sigma(\xi, n) = \frac{2.63 \times 10^{-2} \gamma_E T^{3/2}}{Z} \left[\log \left(\frac{1.23 \times 10^7 T^{3/2}}{Z \sqrt{n_e}} \right) \right]^{-1} \quad (2.23)$$

where Z , given by

$$Z = \frac{x_1 + 4x_2}{x_1 + 2x_2}, \quad (2.24)$$

is a position-dependent number lying between one and two which is indicative of the degree of ionization in the gas and γ_E can be approximated by the value 0.6833. Finally the parameter n_e is the electron density in the gas, viz.,

$$n_e = \frac{\rho(x_1 + 2x_2)}{m_0} \quad (2.25)$$

Equations (2.1), (2.3), (2.6), (2.12), (2.13), (2.14), (2.15), (2.16), (2.17) and (2.22), together with the supplementary information contained in this section, should be sufficient to determine the unknowns J , E , B , p , v_x , v_y , T , ρ , x_1 , x_2 and l_a . In the following section several solutions to these equations are carried out.

7. L. Spitzer, *Physics of Fully Ionized Gases*, (Interscience, New York, 1965), Chap. 5.
8. R.S. Cohen, L. Spitzer, and P. McR. Routly, "The Electrical Conductivity of an Ionized Gas," *Phys. Rev.* 80, 230 (1950).
9. L. Spitzer and R. Harm, "Transport Phenomena in a Completely Ionized Gas," *Phys. Rev.* 89, 977 (1953).

III. SOLUTION OF EQUATIONS

A. General Remarks and Additional Approximations

In Ref. 1 we showed that for a one-dimensional case (no dependence on y) the equations of the preceding section possessed a steady-state solution in which \dot{v} vanished, and we justified the use of that approximation in analyzing the arc's properties. If we make a similar assumption in the two-dimensional analysis, Eqs. (2.6) and (2.13)-(2.15) become

$$w^2 \frac{\partial^2 B}{\partial \xi^2} + \ell_a^2 \frac{\partial^2 B}{\partial \eta^2} = w^2 \frac{\partial \log \sigma}{\partial \xi} \frac{\partial B}{\partial \xi} + \ell_a^2 \frac{\partial \log \sigma}{\partial \eta} \frac{\partial B}{\partial \eta} \quad (3.1)$$

$$\frac{\partial P}{\partial \xi} = - \frac{B}{\mu} \frac{\partial B}{\partial \xi} - \rho \ell_a \alpha \quad (3.2)$$

$$\frac{\partial P}{\partial \eta} = - \frac{B}{\mu} \frac{\partial B}{\partial \eta} \quad (3.3)$$

and

$$w \frac{\partial q_x}{\partial \xi} + \ell_a \frac{\partial q_y}{\partial \eta} = \ell_a w j^2 / \sigma \quad (3.4)$$

In these equations, α represents the common acceleration of the arc and projectile, namely,

$$\alpha = \frac{\mu j^2}{2(\rho_{\ell_a} + \rho_{\ell_p})} \quad (3.5)$$

where ρ_{ℓ_p} is the projectile density multiplied by its length along the x axis.

Equation (3.1) is to be solved subject to the boundary conditions

$$B(0, \eta) = \mu j$$

$$B(1, \eta) = 0 \quad \left(\frac{\partial B}{\partial \eta} \right)_{\eta=0} = \left(\frac{\partial B}{\partial \eta} \right)_{\eta=1} = 0 \quad (3.6)$$

The conditions on B are easily derived from Ampère's law, whereas those on $\frac{\partial B}{\partial \eta}$ are necessary in order that the x component of the current density vanish at the rail-arc interface; otherwise, the associated electric field would produce an infinite current in the perfectly conducting rails. The conditions obeyed by P and T are

$$P(0, \eta) = 0$$

$$T(0, \eta) = T(1, \eta) = T(\xi, 0) = T(\xi, 1) = T_b. \quad (3.7)$$

The latter condition, that the arc is in contact with a thermal reservoir at temperature T_b , is somewhat different from the boundary condition employed in the calculations in Ref. 1. As has been discussed previously, however, the results should be relatively independent of boundary temperature and the latter condition is somewhat easier to treat in the analysis which follows. This point is discussed further in Sec. III C.

If we now integrate Eq. (3.2) and employ Eqs. (3.6) and (3.7), we find

$$P = -\frac{B^2}{2\mu} - \ell_a \alpha \int_0^\xi \rho \, d\xi + \frac{\mu j^2}{2}. \quad (3.8)$$

Substituting Eq. (3.8) into Eq. (3.3) leads us to the conclusion that a steady solution exists only if ρ is independent of η (one-dimensional limit) or for vanishingly small values of the acceleration α . The physical reason that no steady solution (with the gas at rest) can be found is that there exists an effective force on the arc arising from the last term on the right-hand side of Eq. (3.2). Although this force lies along the x direction, it will produce a torque on the arc if the density varies in the y direction and will set the arc in rotational motion.

Including this rotational motion of the arc, as well as possible time-dependent effects, greatly complicates the problem. Therefore, as a first approximation, we will neglect the effect of the arc's acceleration upon its fluid-dynamical properties, set $\alpha = 0$ in Eq. (3.8), and find the steady solution. Consequently, the solution which follows corresponds physically to a situation in which the projectile is held fixed, but the accelerating current is allowed to flow. The nature of the approximation is discussed in greater detail in Sec. IV.

Making use of the approximation discussed above then, we find from Eq. (3.8)

$$P = -\frac{B^2}{2\mu} + \frac{\mu j^2}{2} \quad (3.9)$$

and this result satisfies Eq. (3.3) automatically. In the most general case, no additional simplification of the equations results. However, if the conductivity can be approximated by a separable function of ξ and η so that

$$\sigma(\xi, \eta) = \sigma_x(\xi) \sigma_y(\eta), \quad (3.10)$$

Eq. (3.1) can be solved by separation of variables. We find

$$B = \mu j \int_{\xi}^1 \sigma_x(\xi) d\xi / \int_0^1 \sigma_x(\xi) d\xi . \quad (3.11)$$

Remarkably, the result is independent of η and is identical to the solution obtained in our previous one-dimensional calculations. We also find from Eqs. (2.1) and (2.3)

$$\vec{J} = \frac{j \sigma_x}{l_a \int_0^1 \sigma_x d\xi} \hat{a}_y \quad (3.12)$$

and

$$\vec{E} = \left[\frac{j}{\sigma_y l_a \int_0^1 \sigma_x d\xi} + \mu j v_0 \int_{\xi}^1 \sigma_x d\xi / \int_0^1 \sigma_x d\xi \right] \hat{a}_y . \quad (3.13)$$

Therefore, for the special case in which the plasma conductivity can be approximated as indicated in Eq. (3.10), the following situation exists. The magnetic induction varies only in the direction of propagation and no transverse currents exist. Furthermore, although the conductivity is a function of η , the electric-field intensity also depends on η and in such a way that the current density is independent of η . Considerable simplification results in the numerical solution of the equations if the approximation above is made and for the problem at hand, as we shall see, the approximation is not unreasonable. We now turn to a solution of the equations in several cases of interest.

B. Limiting-Case Analytic Solution

Although we will be concerned primarily with the numerical solution of the governing equations for reasonably general cases, it is nonetheless of interest to carry out a limiting-case analytic solution. Such a solution is useful for checking the computational results for the more general cases, for providing some physical insight into the nature of the solution, and for obtaining some approximate scaling relations which will be discussed presently. In order to make the analysis possible we neglect the position dependence of the plasma conductivity, radiation mean free path, and degree of ionization (i.e., x_1 and x_2). Despite the apparent lack of justification for these assumptions, the analytic results will be seen to be in agreement with the more general numerical results to within at least a few percent.

Under the assumptions discussed above, we have from Eq. (3.11)

$$B = \mu j (1-\xi), \quad (3.14)$$

and from Eq. (3.9),

$$P = \mu j^2 (\xi - \xi^2/2) . \quad (3.15)$$

The current density, J , then follows directly from Eq. (3.12), namely,

$$J = j/\ell_a . \quad (3.16)$$

Using Eqs. (2.20) and (3.16) in the energy equation, Eq. (3.4), we find

$$\frac{1}{\ell_a^2} \frac{\partial^2 t}{\partial \xi^2} + \frac{1}{w^2} \frac{\partial^2 t}{\partial \eta^2} + \frac{3j^2}{4\sigma_S \sigma \lambda \ell_a^2} = 0 \quad (3.17)$$

where

$$t = T^4 . \quad (3.18)$$

The solution to Eq. (3.17) can be written

$$T^4(\xi, \eta) = T_b^4 + \frac{3j^2 w}{16\pi \sigma_S \sigma \lambda \ell_a} \int_0^1 d\xi' \int_0^1 d\eta' G(\xi, \eta; \xi', \eta') \quad (3.19)$$

where G is the Green function for a rectangular surface. One has¹⁰

$$G(\xi, \eta; \xi', \eta') = \frac{16}{\pi \ell_a w} \sum_{k,p=1}^{\infty} \frac{\sin(k\pi\xi) \sin(k\pi\xi') \sin(p\pi\eta) \sin(p\pi\eta')}{(k^2/\ell_a^2 + p^2/w^2)} . \quad (3.20)$$

Carrying out the integration, we find

$$T = T_b \left[1 + \frac{12j^2}{\pi^4 \sigma_S \sigma \lambda T_b^4} \sum_{k=1,3,5}^{\infty} \sum_{p=1,3,5}^{\infty} \frac{\sin(k\pi\xi) \sin(p\pi\eta)}{kp(k^2 + p^2 \ell_a^2/w^2)} \right]^{1/4} . \quad (3.21)$$

The mass density then follows directly from Eq. (2.16) and (3.15),

$$\rho = \frac{m_0 \mu j^2 (\xi - \xi^2/2)}{(1 + x_1 + 2x_2) k_B T} , \quad (3.22)$$

with T given by Eq. (3.21). In principle, Eq. (3.22) can now be substituted into Eq. (2.22) and the resulting integral evaluated. That result would then be used in conjunction with Eqs. (3.21) and (3.22) to determine the unknowns

10. R. Courant and D. Hilbert, Methods of Mathematical Physics (Interscience, New York, 1953), Vol. I, Chap. V.

T , ρ , and ℓ_a independently. In practice the resulting integral cannot be evaluated nor can ℓ_a be separated from the infinite series in Eq. (3.21). Therefore, a numerical solution is necessary even in solving the equations resulting from this analytic treatment. In two special cases, however, an exact analytic solution can be found and we now consider these cases.

1. Case I: $w \gg \ell_a$ (one-dimensional limit)

For $w \gg \ell_a$, $p^2 \ell_a^2 / w^2$ is negligible with respect to k^2 in Eq. (3.21) for any contributing values of p and k and can be neglected. Furthermore, one can show that

$$\sum_{k=1,3,5}^{\infty} \frac{\sin(p\pi\xi)}{k^3} = \frac{\pi^3}{8} (1-\xi) \quad (3.23)$$

and

$$\sum_{p=1,3,5}^{\infty} \frac{\sin(p\pi\eta)}{p} = \pi/4, \quad (3.24)$$

so Eq. (3.21) becomes

$$T = T_b \left[1 + \frac{3j^2 \xi(1-\xi)}{8\sigma_S \lambda \sigma T_b^4} \right]^{1/4} \quad (3.25)$$

and Eq. (3.22) becomes

$$\rho = \frac{m_0 \mu j^2 (\xi - \xi^2/2)}{(1+x_1+2x_2) k_B T_b \left[1 + \frac{3j^2 \xi(1-\xi)}{8\sigma_S \sigma \lambda T_b^4} \right]^{1/4}} \quad (3.26)$$

The arc length ℓ_a can be calculated now by substituting Eq. (3.26) into Eq.

(2.22) and evaluating the resulting integral. For purposes of carrying out the integration, the first term in brackets in Eq. (3.26) is neglected with respect to the second since the latter term dominates except very close to $\xi = 0$ and $\xi = 1$. We find

$$\ell_a = \frac{20 (1+x_1+2x_2) k_B \rho \ell_a \Gamma(1/2)}{13 m_0 \mu j^{3/2} (8\sigma_S \sigma \lambda / 3)^{1/4} \Gamma^2(3/4)} \quad (3.27)$$

where Γ is the gamma function; the ratio $\Gamma(1/2)/\Gamma^2(3/4)$ is about 1.2. Therefore, Eqs. (3.14), (3.15), (3.25), (3.26), and (3.27) provide uncoupled expressions for B , p , T , ρ and ℓ_a .

2. Case II: $w \ll \ell_a$

The assumption that $w \ll \ell_a$ is the one most frequently encountered in experiments of interest. Under this condition k^2 can be neglected with respect to $p_a^2 \ell_a^2 / w^2$ in Eq. (3.21) and, using Eqs. (3.23) and (3.24) as before, we find

$$T = T_b \left[1 + \frac{3j^2 \eta (1-\eta) w^2}{8\sigma_S \sigma \lambda T_b^4 \ell_a^2} \right]^{1/4} \quad (3.28)$$

and

$$\rho = \frac{m_0 \mu j^2 (\zeta - \xi^2/2)}{(1 + x_1 + 2x_2) k_B T_b \left[1 + \frac{3j^2 \eta (1-\eta) w^2}{8\sigma_S \sigma \lambda T_b^4 \ell_a^2} \right]^{1/4}} \quad (3.29)$$

Similarly, calculating the arc length as before, we have

$$\ell_a = \frac{3 (1 + x_1 + 2x_2) k_B \rho \ell_a \Gamma(1/2) w^{1/2}}{2m_0 \mu j^{3/2} (8\sigma_S \sigma \lambda / 3)^{1/4} \Gamma^2(3/4) \ell_a^{1/2}},$$

whence

$$\ell_a = \left[\frac{3 (1 + x_1 + 2x_2) k_B \rho \ell_a \Gamma(1/2)}{2m_0 \mu \Gamma^2(3/4)} \right]^{2/3} \frac{w^{1/3}}{j (8\sigma_S \sigma \lambda / 3)^{1/6}} \quad (3.30)$$

Equation (3.30) can now be substituted into Eq. (3.28) to produce T and into Eq. (3.29) to produce ρ .

3. Comparison of Two Solutions

It is interesting to compare the solution obtained in Sec. B.1 (one-dimensional case) with that obtained in Sec. B.2 (two-dimensional case) in the light of our remarks in Sec. I concerning the expected differences in the two calculations. Thus, we see that in this simplified case identical expressions are obtained for the pressure P and magnetic induction B . For a constant arc length ℓ_a , however, the temperature in the interior of the arc is smaller in the two-dimensional case than that in the one-dimensional case by a factor which decreases with increasing arc length. The latter result can be seen by comparing Eqs. (3.25) and (3.28) in the preceding analysis.

C. Numerical Technique

In the remainder of this section we will discuss more general solutions to the governing equations for several cases. In particular, it will no longer be assumed that the conductivity, mean free path, and degree of ionization are uniform in the arc but, rather, their spatial dependence will be accounted for. Because of the additional complication introduced, we must resort to numerical solutions of the equations, and the particular numerical procedure is described in this section.

We first noted that the previous one-dimensional results suggested that substantial variations in the flow parameters could be expected very near the projectile surface, i.e., in the vicinity of $\xi = 1$. This problem was dealt with in the one-dimensional treatment by simply making the step size small. In two dimensions, however, such a remedy is not practical. Instead, we performed a "stretching transformation" by letting

$$\xi = 1 - \xi'^2, \quad (3.31)$$

and solved the equations as a function of ξ' . As can be easily seen, for constant $\Delta\xi'$ such a transformation has the effect of decreasing the step size near $\xi = 1$ where rapid variations occur, and of increasing the step size near $\xi = 0$ where variations are slower.

We then employed an iterative technique similar to that used in our previous one-dimensional calculations. Specifically, we divided the $\xi'\eta$ plane into a grid and approximated all derivatives by finite differences. The resulting coupled equations were then written in the form

$$V_k(i,j) = F(V_1, V_2 \dots V_k' \dots V_N; \xi'\eta) \quad (3.32)$$

where $V_k(i,j)$ denotes the k^{th} unknown (P, T , etc.) at the $(i,j)^{\text{th}}$ point and where F denotes some function of the remaining unknowns, ξ' , and η . The prime on V_k in the argument of F denotes that $V_k(i,j)$ does not appear on the right-hand side of the equation. Initial values for the variables on the right-hand side of the equations were obtained from the analytic approximation discussed in Sec. IIIB, and new values were calculated on the left-hand sides. For the second iteration, a weighted average of the old and new values was used on the right-hand sides. The process was then repeated and was found to converge in a few hundred iterations.

We have performed calculations in which we used the general expression for the plasma conductivity in Eq. (2.23), as well as calculations in which we made the separable-conductivity approximation in Eq. (3.10). In the latter case, σ_x and σ_y were obtained from the relations

$$\sigma_x(\xi) = \int_0^1 \sigma(\xi, \eta) d\eta / \langle \sigma(\xi, \eta) \rangle^{1/2} \quad (3.33)$$

$$\sigma_y(\eta) = \int_0^1 \sigma(\xi, \eta) d\xi / \langle \sigma(\xi, \eta) \rangle^{1/2} \quad (3.34)$$

where $\sigma(\xi, \eta)$ is given by Eq. (2.23) and where the brackets denote an average taken over the entire arc. In all these calculations we monitored both the actual and the factored conductivity and good agreement was found between the two expressions in all cases. Presumably, the reason for the excellent agreement is that the conductivity is a very slowly varying function in the interior of the arc, and varies rapidly only with ξ or η , but not both, near the boundaries. The advantage of using the factored conductivity is that the iterative procedure converges far more rapidly than in the more general case, no doubt because of the absence of small transverse currents. In most of the remainder of the discussion we will confine ourselves to results in which the separable-conductivity approximation was made. In Sec. IV, however, some qualitative results of the more general case are discussed.

We have performed calculations using a variety of step sizes for $\Delta\xi'$ and $\Delta\eta$ and have found that the values $\Delta\xi' = \Delta\eta = 0.02$ gave acceptable results in a reasonable calculation time. When $\Delta\xi'$ or $\Delta\eta$ was increased by a factor of two, for example, we observed changes in some variables by as much as 3 or 4% from results obtained at the smaller step size. Most quantities were in substantially better agreement than that, however, and we assumed that values of $\Delta\xi'$ and $\Delta\eta$ given by 0.02 were sufficiently small.

As has been emphasized before, the fluid-dynamic variables within the arc are nearly independent of T_b provided the boundary temperature is small with respect to the maximum temperature within the arc. Under these conditions the arc temperature is determined by the rate of energy dissipation only, and the boundary temperature has negligible effect. On the other hand, in the numerical calculations it is desirable to have the boundary temperature as large as possible in order to avoid numerical difficulties that may arise from steep temperature gradients near the boundaries. Therefore, in the numerical calculations we set T_b equal to some fraction of the estimated maximum temperature within the arc, and then lowered the value until further reduction produced no appreciable change in the arc properties. In practice, reasonable values of the boundary temperature were found to be about 50% of the maximum temperature in the arc.

D. Analysis of Rashleigh-Marshall Experiment

In a recent experiment¹¹ Rashleigh and Marshall (RM) have employed an arc-driven rail gun to accelerate a 3-g projectile to about 6 km/s. The arc consisted of partially ionized copper vapor. In an effort to analyze the arc in that experiment, we have solved the two-dimensional equations for determining the arc properties for a set of input data roughly equivalent to the RM data.

The appropriate data are shown in Table I. All quantities were either taken directly from the experimental specifications or easily calculated therefrom. The parameter h is an effective rail height necessary for use in the

11. S.C. Rashleigh and R.A. Marshall, "Electromagnetic Acceleration of Macro-particles to High Velocities," *J. Appl. Phys.* 49, 2540 (1978).

TABLE I. Experimental Data for Rashleigh-Marshall Experiment.

Quantity	Description	Value
w	Rail separation	$1.27 \times 10^{-2} \text{ m}$
h_p	Plasma height on rails	$1.27 \times 10^{-2} \text{ m}$
h_r	Rail height	$1.91 \times 10^{-2} \text{ m}$
h	Effective rail height	$1.56 \times 10^{-2} \text{ m}$
m_p	Projectile mass	$3 \times 10^{-3} \text{ kg}$
i	Pulsed current	$3 \times 10^5 \text{ A}$
j	Current per unit height on rails	$1.92 \times 10^7 \text{ A/m}$
V_0	Muzzle voltage	160 V
m_a	Arc mass	$2 \times 10^{-4} \text{ kg}$
m_0	Ion (or atom) mass	$1.1 \times 10^{-25} \text{ kg}$
a	Average acceleration	$6 \times 10^6 \text{ m/s}^2$
$\rho_{\ell a}$	(See Eq. (3.5))	0.51 kg/m^2
$\rho_{\ell p}$	(See Eq. (3.5))	15.1 kg/m^2

calculations since the quantities h_p and h_r , defined in the table, were assumed to be equal in the model. As can be seen, h was chosen to be the geometric mean of the two experimental values. The arc mass m_a was unknown experimentally but we used a value, found by trial and error, which gave an arc length ℓ_a of about 10 cm. Finally, the experimental quantity V_0 represents the potential measured across the end of the rails. The theoretical value can be obtained from Eq. (3.13) by evaluating the expression at $\xi = 1$ and noting that

$$V_0 = w \int_0^1 E(1, n) \, dn \quad (3.35)$$

Typical results obtained from the numerical calculation are shown in Table II for quantities which are independent of position. The acceleration a is about a factor of two and one-half higher than the experimental value of $6 \times 10^6 \text{ m/s}^2$. The lack of agreement no doubt results because the use of infinitely high rails overestimates the acceleration imparted to the projectile, and

TABLE II. Results of Numerical Calculations for Rashleigh-Marshall Experiment

Quantity	Value
a	$1.5 \times 10^7 \text{ m/s}^2$
l_a	9.8 cm
$\langle Z \rangle$	1.61
$\langle T \rangle$	$3.7 \times 10^4 \text{ }^\circ\text{K}$
$\langle n_e \rangle$	$1.4 \times 10^{26} \text{ m}^{-3}$
V_0	50 volts

because of the somewhat arbitrary manner in which the effective height h was chosen. In a similar manner the calculated potential V_0 is about a factor of three lower than the experimental value shown in Table I.

The remaining quantities in the table are largely self evident. It is of interest, however, to compare them with the corresponding results obtained in the previous one-dimensional treatment for an arc of roughly the same length. As expected, we find that the mean temperature of $37,000^\circ\text{K}$ is substantially lower than for the one-dimensional case in which we found $\langle T \rangle \approx 57,000^\circ$. As a result of the lower temperature, the mean ionization $\langle Z \rangle$ is also lower than the one-dimensional value of 1.93. Since the pressure should be nearly the same in the two calculations, as we indicated before, the mass density in the arc should be higher than in the one-dimensional case in order to satisfy the equation of state and, therefore, the electron density is also higher. Thus, we found $\langle n_e \rangle = 9.9 \times 10^{25} \text{ m}^{-3}$ in our previous treatment and this value is indeed smaller than the present value of $1.4 \times 10^{26} \text{ m}^{-3}$. Finally, we observe that the potential V_0 is roughly the same in the two calculations (50 volts compared to 47 volts). It is perhaps surprising that the potential is not significantly higher than that in the one-dimensional case since the conductivity of the arc varies as $T^{3/2}$. However, in this particular temperature range, the degree of ionization is also smaller and there are, consequently, fewer collisions among the electrons. The reduced scattering tends to increase the conductivity and this effect nearly compensates for the effect of the reduced temperature. Thus, little change in the conductivity results.

Graphs of the position-dependent quantities are shown in Figs. 2-6. For the pressure and magnetic induction, graphs are drawn as a function of ξ . These quantities do not depend on η when the conductivity is approximated by a separable function, and only weakly so when the more general expression is used. This behavior, incidentally, is indicative of our earlier statement that only small differences between these parameters should be expected in the one- and two-dimensional calculations.

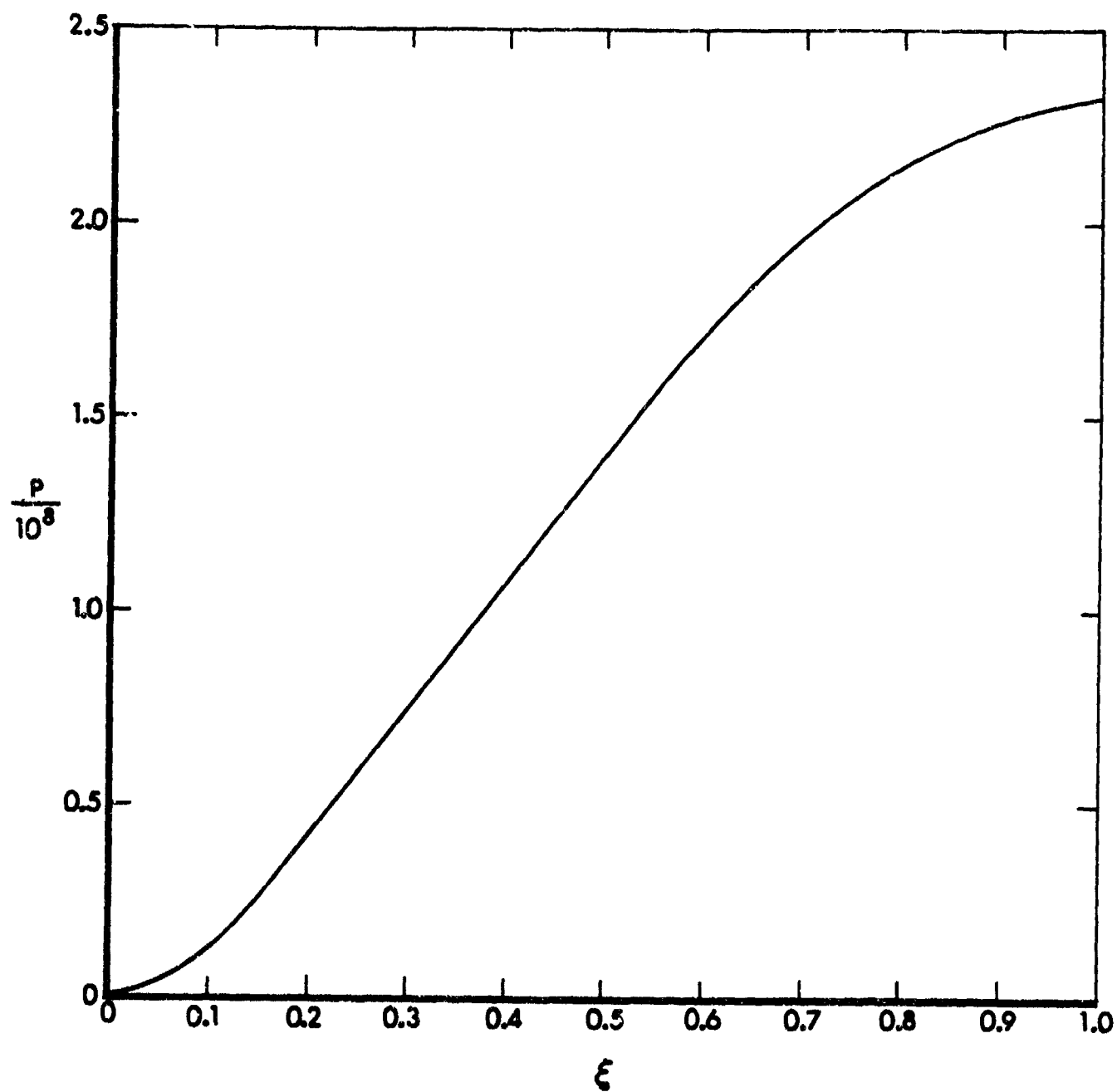


Figure 2. Pressure, in Pascals, as a Function of ξ .

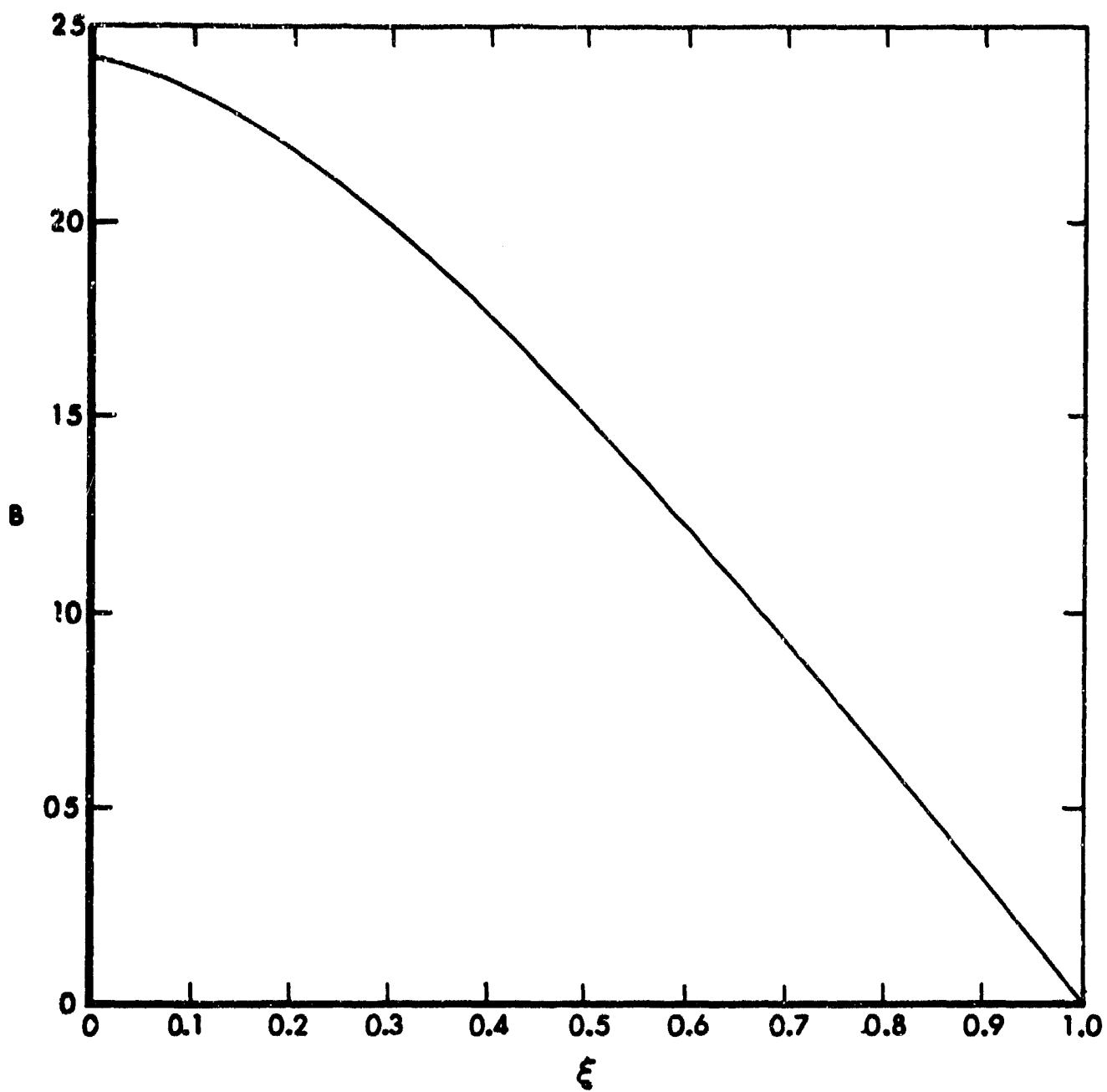


Figure 3. Magnetic Induction Field, in Tesla, as a Function of ξ .

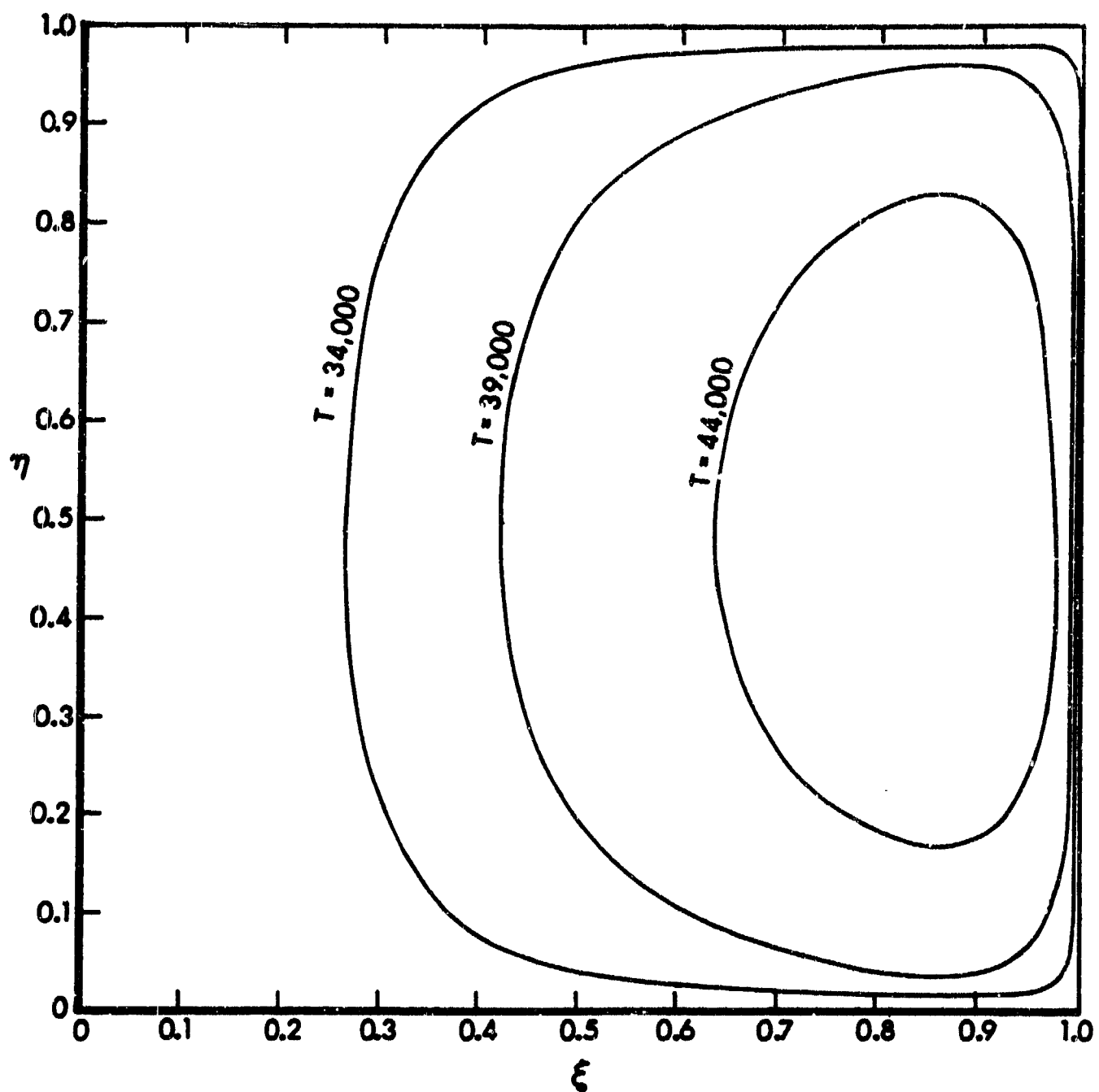


Figure 4. Lines of Constant Temperature, in Degrees Kelvin, Within the Arc.

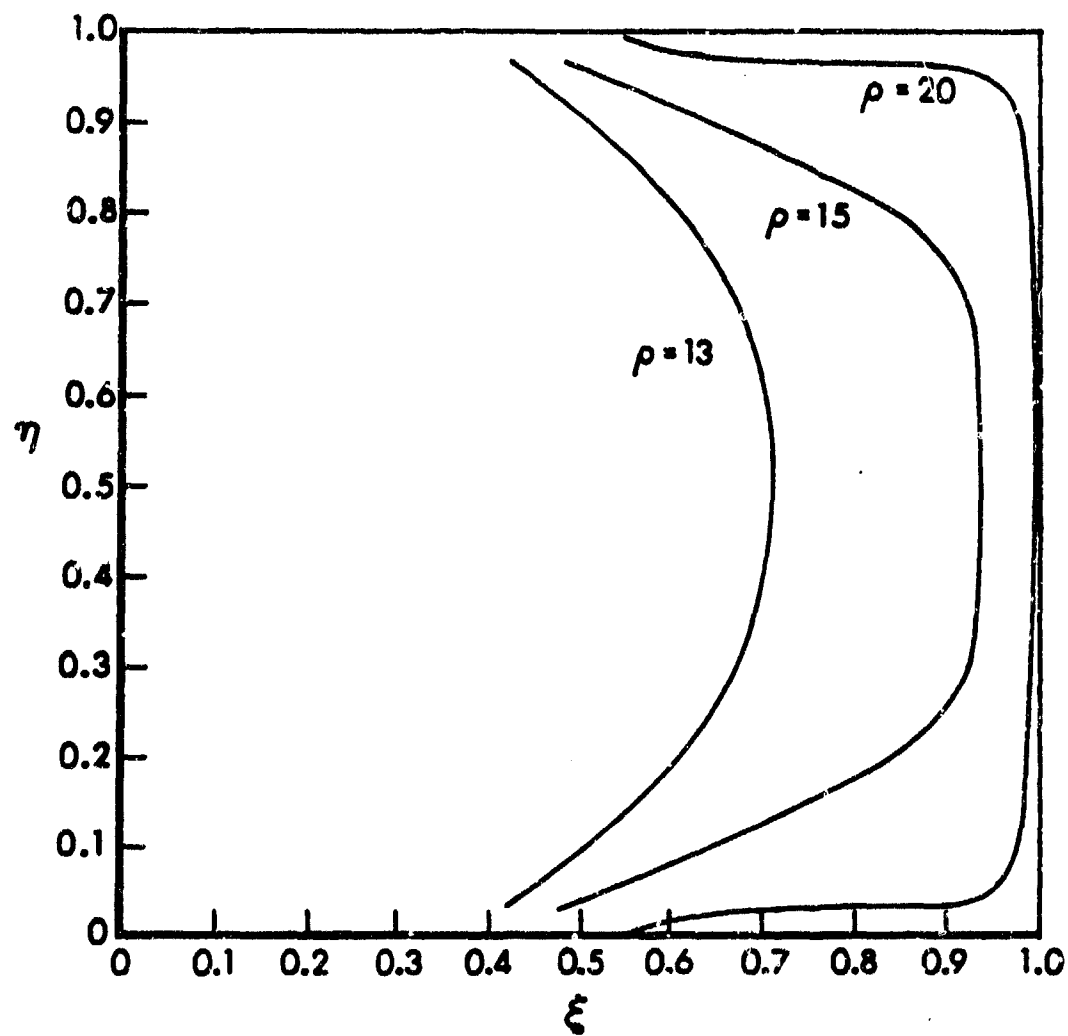


Figure 5. Lines of Constant Mass Density, in kg/m^3 , Within the Arc.

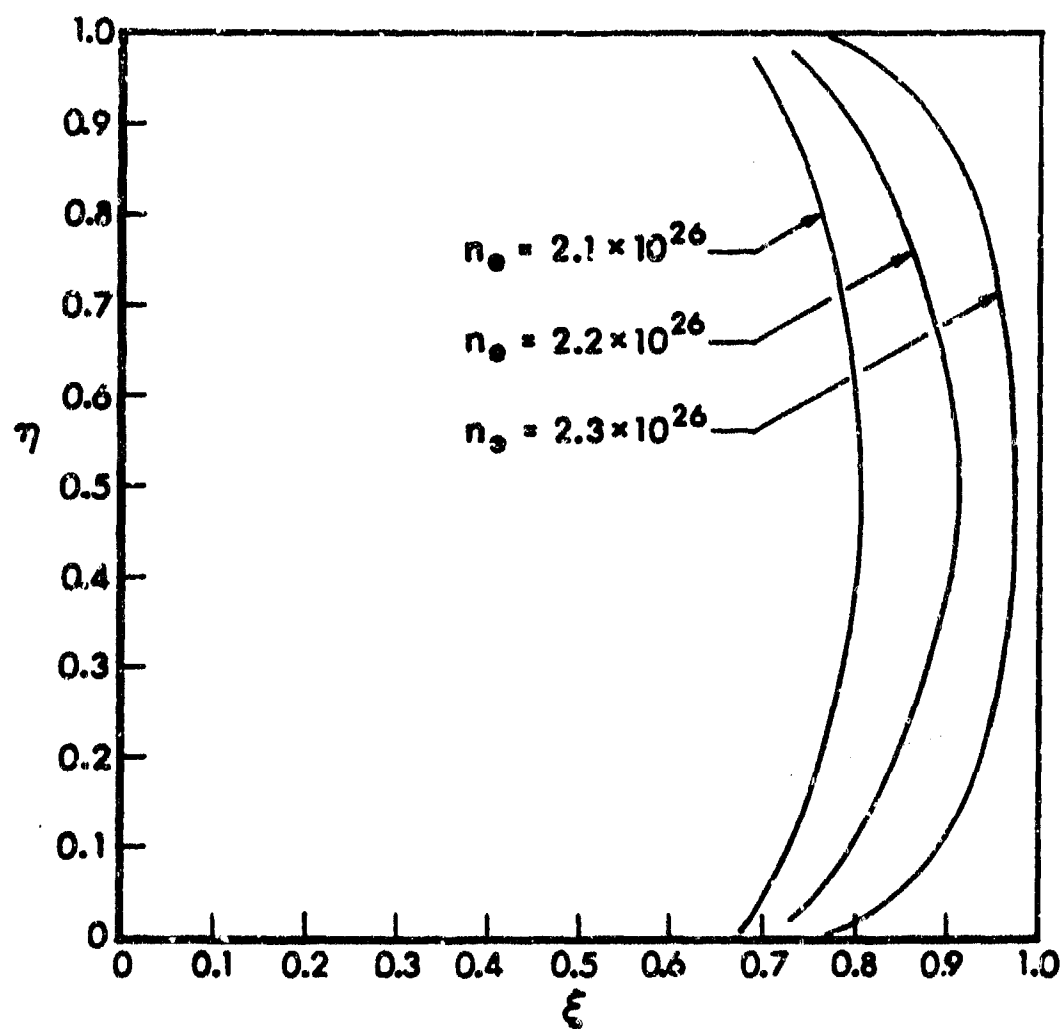


Figure 6. Lines of Constant Electron Density, in m^{-3} , Within the Arc.

The pressure, shown in Fig. 2, rises monotonically from zero at the back of the arc to about 220 MPa at the projectile surface. Its functional dependence may be compared with the approximate analytic form in Eq. (3.15). Similarly, the magnetic induction field varies from about 24 Tesla at the trailing edge of the arc to zero at the projectile surface. If the conductivity of the arc were constant, the variation between these two values would be linear. The fairly weak dependence of the conductivity on position, however, gives rise to the small deviations from linear behavior observed in the graph.

In Fig. 4, two-dimensional effects of the temperature profile are shown by plotting isotherms within the arc. Here, unlike for the pressure and fields, significant variations of the temperature were observed as a function of η , particularly near the surface of the rails. It may furthermore be noted that there is a high concentration of energy near the projectile surface, with a very steep gradient as the surface is approached. The high temperature near the surface can be explained by noting that there is an increase in mass density with increasing ξ (see Fig. 5) and, consequently, a decrease in the radiation mean free path. Thus, photons created in the right-most part of the arc are radiated away with more difficulty than those in the left-most part. Once the photons are within a mean free path or so of the boundary, however, they can essentially "see" the boundary and are easily radiated outward. Therefore, the temperature drops rapidly very near the projectile surface. The maximum temperature in the arc was found to be about 46,000°K whereas in our previous one-dimensional work the maximum was observed to be about 70,000 deg. As noted earlier, the temperature was expected to be smaller for the two-dimensional calculation.

In Fig. 5 are plotted lines of constant mass density. The density may be seen to vanish at the back of the arc and, as in the temperature plot, a rather rapid variation in the density is observed near the projectile surface. The increase there results because, as the temperature falls, the degree of ionization also falls, and both these effects tend to reduce the pressure at the projectile surface. Therefore, a steady pressure can be maintained at the surface only if there is a proportionate increase in density there.

Finally, lines of constant electron density may be observed in Fig. 6. The curves are similar to those for the mass density but the gradient near $\xi = 1$ is significantly less pronounced. The reason for the smaller gradient, of course, is that the ions near the projectile surface are less highly ionized than those in the interior of the arc because of the lower temperature.

E. Analysis of Westinghouse Experiment

In addition to the analysis of the arc in the Rashleigh-Marshall experiment, we have also performed calculations to determine the properties of an arc for a rail gun comparable in size to that under construction at Westinghouse. Typical input parameters, again taken largely from the experimental specifications, are shown in Table III. As in the RM case, the parameter $\rho_{\ell a}$ was chosen by trial and error to produce an arc length of roughly ten centimeters; the pulsed current i was chosen so as to produce an acceleration sufficient for the projectile to reach a velocity of 3 km/s in a distance of 4m.

TABLE III. Experimental Data for Westinghouse Gun.

Quantity	Description	Value
w	Rail separation	5.0×10^{-2} m
h	Rail height	5.0×10^{-2} m
m_p	Projectile mass	0.3 kg
i	Pulsed current	7.35×10^5 A
j	Current per unit height on rails	1.47×10^7 A/m
m_a	Arc mass	1.2×10^{-3} kg
$\rho_{\ell a}$	(See Eq. (3.5))	0.48 kg/m^2
$\rho_{\ell p}$	(See Eq. (3.5))	120 kg/m^2

Position-dependent quantities in the calculation vary in essentially the same manner as for the RM case, so the significant results will be presented only in tabular form. These results are shown in Table IV. The results

TABLE IV. Results of Numerical Solution for Westinghouse Gun.

Quantity	Value
α	$1.13 \times 10^6 \text{ m/s}^2$
ℓ_a	9.9 cm
V_0	171 volts
$\langle T \rangle$	4.2×10^4 °K
T_{\max}	5.2×10^4 °K
$\langle n_e \rangle$	$8.0 \times 10^{25} \text{ m}^{-3}$
$n_{e \max}$	$1.6 \times 10^{26} \text{ m}^{-3}$
ρ_{\max}	17.0 kg/m^3
$\langle Z \rangle$	1.83
P_{\max}	1.4×10^8 Pa
B_{\max}	18.4 T

should be compared with those in both Table II and in Figs. 2-6. The magnitudes of the various flow parameters are sufficiently similar to those obtained in the RM experiment to suggest that no major difficulties should be expected in using an arc armature in this larger gun. It is interesting to note, however, that the two-dimensional model predicts a slightly higher temperature for the large-gun arc than for the RM arc, the opposite of the prediction in the one-dimensional case. The reasons for the contradictory predictions as well as some other results of the calculation will be made clearer in the following section where some approximate scaling laws will be derived.

F. Scaling Relations and Optimum Arc Materials

The numerical calculations undertaken previously are difficult to carry out and computationally rather inefficient. It is of interest, therefore, to attempt to derive some approximate scaling relations which indicate how arc characteristics vary with experimental parameters. Such a set of relations can be derived from the special-case analytic solution presented in Sec. IIIB if some additional assumptions are made, and if either $\ell_a \ll w$ or $\ell_a \gg w$. In particular, we make the following additional approximations: (1) In order to account to some extent for the temperature dependence of the conductivity in the results of Secs. IIIB.1 and IIIB.2, we assume

$$\sigma \propto T^{3/2}/Z \quad (3.36)$$

and neglect the logarithmic term in Eq. (2.23). (2) We note that the radiation mean free path λ in Eq. (2.21) varies approximately according to the relation⁶

$$\lambda \propto \frac{m_0^2 T^{7/2}}{\rho^2 \langle j \rangle (\langle j \rangle + 1)^2} \quad (3.37)$$

where $\langle j \rangle$ for this case can be approximated by

$$\langle j \rangle = x_1 + 2x_2 \quad (3.38)$$

(3) Finally, we note that the parameter $\langle j \rangle$ can be well approximated by the parameter Z (see Eq. (2.24) if either single or double ionization is dominant. In order to simplify the results as much as possible, we will assume this to be the case.

If we make use of the assumptions noted above in the results of Secs. IIIB.1 and IIIB.2 and solve the coupled equations for the unknown quantities, we obtain the scaling relations indicated in Table V. The results should be reasonably valid provided they are applied not too close to the arc's boundaries. In order to use the table to predict some quantity of interest for a case

TABLE V. General Scaling Factors .

Quantity	$\lambda_a \ll w$ (1D Limit)	$\lambda_a \gg w$
B	j	j
P	j^2	j^2
α	$j^2 / (\rho_{\ell p} + \rho_{\ell a})$	$j^2 / (\rho_{\ell p} + \rho_{\ell a})$
T	$j^{6/11} Z^{2/11}$	$\frac{j^{10/13} w^{2/13} Z^{2/13} m_0^{2/13}}{(1+Z)^{2/13} \rho_{\ell a}^{2/13}}$
ρ	$\frac{m_0 j^{16/11}}{(1+Z) Z^{2/11}}$	$\frac{m_0^{11/13} j^{16/13} \rho_{\ell a}^{2/13}}{w^{2/13} Z^{2/13} (1+Z)^{11/13}}$
λ_a	$\frac{\rho_{\ell a} (1+Z) Z^{2/11}}{m_0 j^{16/11}}$	$\frac{\rho_{\ell a}^{11/13} w^{2/13} Z^{2/13} (1+Z)^{11/13}}{m_0^{11/13} j^{16/13}}$
V	$\frac{w j^{18/11} Z^{6/11} m_0}{\rho_{\ell a} (1+Z)}$	$\frac{w^{8/13} Z^{8/13} j^{14/13} m_0^{8/13}}{\rho_{\ell a}^{8/13} (1+Z)^{8/13}}$
n_e	$\frac{j^{16/11} Z^{9/11}}{(1+Z)}$	$\frac{j^{16/13} \rho_{\ell a}^{2/13} Z^{11/13}}{w^{2/13} m_0^{2/13} (1+Z)^{11/13}}$

in which no numerical calculations exist, the following procedure is followed. The value of a particular quantity in the RM experiment (column 1) is multiplied by ratio of the scaling factors for the unknown and RM cases. The result, then, is the value of the parameter of interest in the unknown case. The degree of ionization, Z , is not easily expressible as a function of the experimental quantities as are the other unknowns. Fortunately, however, large changes in this parameter do not occur even with fairly significant changes in the experimental conditions, and it can often be treated as a constant in the two cases of interest.

The results in Table V are general and, except for their dependence on Z , depend only on the experimental conditions. In the calculations undertaken so far, however, we have varied the experimental parameter, ρ_{ℓ_a} , in order to maintain a constant arc length of roughly 10 cm. It is, therefore, of interest to determine scaling relations as a function of arc length and treat ℓ_a as an experimentally determined quantity. To do so, we solve for ρ_{ℓ_a} in terms of ℓ_a (see the sixth entry in Table V) and substitute the result elsewhere in the table. We then obtain the results shown in Table VI.

TABLE VI. Scaling Factors as a Function of Arc Length.

Quantity	$\ell_a \ll w$	$\ell_a \gg w$
B	j	j
P	j^2	j^2
α	$j^2 / (\rho_{\ell_a} + \rho_{\ell_p})$	$j^2 / (\rho_{\ell_a} + \rho_{\ell_p})$
T	$j^{6/11} Z^{2/11}$	$j^{6/11} Z^{2/11} (w/\ell_a)^{2/11}$
ρ	$\frac{m_0 j^{16/11}}{(1+Z) Z^{2/11}}$	$\frac{m_0 j^{16/11}}{(1+Z) Z^{2/11}} (\ell_a/w)^{2/11}$
V_0	$\frac{w j^{2/11} Z^{8/11}}{\ell_a}$	$\frac{w j^{2/11} Z^{8/11}}{\ell_a} (\frac{\ell_a}{w})^{3/11}$
n_e	$\frac{j^{16/11} Z^{9/11}}{(1+Z)}$	$\frac{j^{16/11} Z^{9/11}}{(1+Z)} (\frac{\ell_a}{w})^{2/11}$

To demonstrate the application of the table we have used it to determine approximate results for the Westinghouse experiment, using the numerical results for the RM case. Shown in column 2 of Table VII are numerical results for the RM experiment. In column three we have repeated, for convenience, the numerical results for the Westinghouse case (see Table IV). In column four are numerical values of the scaling-factor ratios (see Tables I, III, and VI). Finally, in column five are the results for the Westinghouse experiment as predicted by the scaling relations. Comparing columns three and five we see that, except for the potential V_0 and the electron density n_e , the agreement is excellent. The lack of agreement in the last two quantities results because they are fairly sensitive functions of Z , and this parameter does change somewhat in the two cases (see Tables II and IV for comparison of actual numerical values). In addition, the condition $\ell_a \gg w$, required for the validity of these relations, is not strictly valid for the case at hand.

TABLE VII. Comparison of Numerical and Scaling-Relation Results for Westinghouse Experiment.

Quantity	RM Results (Numerical)	Westinghouse Results (Numerical)	Scaling-Factor Ratio	Westinghouse Results (Scaling Factors)
a	$1.53 \times 10^7 \text{ m/s}^2$	$1.13 \times 10^6 \text{ m/s}^2$	0.074	$1.13 \times 10^6 \text{ m/s}^2$
V_0	50 volts	171 volts	2.6	130 volts
$\langle T \rangle$	$3.7 \times 10^4 \text{ }^\circ\text{K}$	$4.2 \times 10^4 \text{ }^\circ\text{K}$	1.1	$4.1 \times 10^4 \text{ }^\circ\text{K}$
T_{max}	$4.7 \times 10^4 \text{ }^\circ\text{K}$	$5.2 \times 10^4 \text{ }^\circ\text{K}$	1.1	$5.2 \times 10^4 \text{ }^\circ\text{K}$
$\langle n_e \rangle$	$1.4 \times 10^{26} \text{ m}^{-3}$	$8.0 \times 10^{25} \text{ m}^{-3}$	0.52	$7.3 \times 10^{25} \text{ m}^{-3}$
$n_{e \text{ max}}$	$2.5 \times 10^{26} \text{ m}^{-3}$	$1.6 \times 10^{26} \text{ m}^{-3}$	0.52	$1.3 \times 10^{26} \text{ m}^{-3}$
ρ_{max}	35.4 kg/m^3	17.0 kg/m^3	0.52	18 kg/m^3
P_{max}	$2.3 \times 10^8 \text{ Pa}$	$1.4 \times 10^8 \text{ Pa}$	0.58	$1.3 \times 10^8 \text{ Pa}$
B_{max}	24 T	18 T	0.76	18T

Finally, it is of interest to ask what the scaling relations predict concerning the optimum materials to use for the arc. In particular, it has been suggested in the past that it might be desirable to use some substance that is more easily ionized than copper, say potassium or cesium, and attempt to obtain equivalent conductivity at substantially lower temperatures. Unfortunately, as can be seen from Table VI, use of these substances having low ionization potentials will probably not make any appreciable difference in the final temperature of the arc. The reason is that temperatures associated with the arc in any practical experiment are always sufficiently high that almost complete ionization of the arc is obtained. Once the condition has been achieved, additional increases in the electron density, which would accompany lower ionization potential, do not result in higher conductivity and lower temperatures. In fact, as can be seen from Eq. (2.23), as Z becomes larger, the conductivity actually decreases. Referring to Table VI, it is evident that the temperature is controlled largely by the current and, to a significantly smaller extent, by the length of the arc, the rail separation, and the degree of ionization Z . High currents are, of course, necessary to achieve the high accelerations required so we have little control over this parameter. Very small changes in the temperature can be obtained by varying the other three parameters, however, and it is generally desirable to make the length of the arc as long as possible, the rail separation as small as possible, and to choose as the arc material a substance having a high second-ionization potential. Again, however, making the optimum choices is not going to change the temperature significantly as is evident from the table. Doubling the arc length, for instance, for a situation in which Z is held constant, results in a temperature reduction of only about 12%.

To demonstrate the validity of these remarks, we have also performed some numerical calculations for the RM gun using potassium vapor for the arc, rather than the copper vapor used previously. The first and second ionization potentials for potassium are 4.3 eV and 31.8 eV, respectively, and its atomic mass is 39. Corresponding values for copper are 7.7 eV, 20.3 eV, and 64. For constant arc length (~ 10 cm), very small differences were noted in the temperature in the two calculations. In fact, the only parameter in Table VI which changed more than a few percent was the mass density ρ . It was found to be about a factor of two smaller for the potassium arc than for the copper arc. The result is predictable from Table VI and can be ascribed to the smaller atomic mass, m_0 , for potassium.

IV. DISCUSSION

In Ref. 1 we discussed in some detail the assumptions employed in the one-dimensional calculation. For the most part, that discussion applies to the two-dimensional case as well. Therefore, in this section we will confine ourselves to summarizing the results of the two-dimensional calculation and to discussing only assumptions pertinent to that case.

We have derived a general, time-dependent formalism for studying arc dynamics in two dimensions. For purposes of carrying out the calculation, we have neglected the effect of the arc's acceleration upon its fluid-dynamical characteristics, and have assumed that those characteristics are steady in a frame

of reference moving with the arc. The latter assumption was also made in our previous one-dimensional treatment. The resulting governing equations were then solved to analyze the arcs both in the RM experiment and for a gun comparable in size to that under construction at Westinghouse. From approximate analytic solutions to the governing equations, some approximate scaling relations were derived and these relations were shown to yield results in reasonably good agreement with the more general numerical solutions.

The assumption that α is negligible in the governing equations may be viewed as the lowest-order approximation in any of an infinite number of perturbation-expansion solutions, valid for small values of the acceleration. For example, if one assumes that all the time-derivative terms in the equations (including the velocities) are small, as in a quasi-static approximation, a reasonably straightforward expansion of the equations can be obtained, with the equations actually solved corresponding to lowest order. Higher-order approximations can also be written down in such an expansion, but the results quickly become quite tedious.¹² At any rate, it is clear that there is no steady solution in higher orders of the two-dimensional problem for a situation in which the gas is at rest relative to the projectile. This situation may be contrasted with the one-dimensional case where such an expansion may also be carried out. In this instance, however, one finds a steady solution to the governing equations in all the higher orders. Moreover, it is also found¹² in this case that the lowest-order terms are an excellent approximation to the exact solutions; the two results differ by only a few percent.

We should also point out that a steady solution may exist in the two-dimensional case for a situation in which the arc is in motion relative to the projectile, provided that motion is itself steady. One might envision, for example, two counter-rotating flows in the arc with the velocity as a function of position remaining constant in time. The counter-rotation is necessary, of course, to conserve the arc's total angular momentum.

It is of some interest to attempt to estimate the conditions under which the velocity might be expected to be small in such a situation. To do so, we first of all note that $\rho \sim \rho_a / L$, where L is some distance characteristic of the arc dimensions, whereas P and the field-dependent terms in Eqs. (2.13) and (2.14) are of the order of $\rho_a \alpha$. Consequently, one can neglect the term $\rho_a \omega a$, as well as terms containing v'_x and v'_y , in the momentum-conservation equations provided $\rho_a / \rho_p \ll 1$. This condition is satisfied in most cases of interest. In order to determine the conditions under which the "rotational" velocities v'_x , and v'_y are negligible in the energy equation, Eq. (2.15), we assume

12. Author's unpublished calculations.

$$x_1 + 2x_2 \sim 2$$

$$e \sim 9k_B T / 2m_0 \quad (4.1)$$

$$J \sim j/L$$

$$\Delta T \sim T/2, \quad (4.2)$$

where ΔT represents the change in T in a distance comparable to L . Using these assumptions, along with Eqs. (2.16) and (2.20), we estimate from Eq. (2.15) that

$$T \sim \left(\frac{3j^2}{2L \sigma_s \sigma \lambda} \right)^{1/4} \left[1 - \frac{7\sigma L \rho_{\ell p} \alpha v_r}{2j^2} \right]^{1/4} \quad (4.2)$$

where v_r stands for rotational velocity. Clearly, to neglect v_r we must have

$$v_r \ll \frac{8j^2}{7\sigma L \rho_{\ell p} \alpha} \quad (4.3)$$

Finally, to determine conditions under which we can neglect rotational velocities for purposes of determining the magnetic-induction field, we assume

$$B \sim \mu j \quad (4.4)$$

and conclude from Eq. (2.6) that we must have

$$v_r \ll (\mu \sigma L)^{-1/2} \quad (4.5)$$

Unfortunately, it is difficult to obtain reliable estimates of v_r . An upper bound is probably some number of the order of

$$v_r \sim (\alpha L)^{1/2}; \quad (4.6)$$

for this value of v_r Eqs. (4.3) and (4.5) are not well satisfied for all cases of experimental interest. It is likely, however, that v_r is sizably smaller than the value suggested in Eq. (4.6) and, for more realistic values of this parameter, Eqs. (4.3) and (4.5) may be easily satisfied. Some further study of this problem, as well as the question of whether a steady state can even exist, is evidently desirable and is deferred to future work.

As pointed out previously, all calculations discussed here are ones for which the separable-conductivity approximation in Eq. (3.10), was made. However, we have also carried out calculations using the more general expression for the conductivity. For these latter calculations, we obtained nonzero values of J_x as well as some η dependence in both B and P. The magnitude of J_x , however, was some four orders of magnitude smaller than that of J_y and the η dependence of both B and P was negligible. These results clearly demonstrate that the separable-conductivity approximation is quite good for the problem at hand; monitoring both the factored and the actual conductivity in our numerical calculations led us to the same conclusion. As a point of academic interest, it is perhaps worth mentioning that the small values of J_x are such that they give rise to a total current density \vec{J} which flows toward regions where the conductivity is high.

In Ref. 1 we pointed out that a one-dimensional model could be expected to substantially overestimate the mean temperature within the arc, because only two surfaces of the arc were available for radiation in such a model. It was pointed out that the mean temperature should vary roughly as $A^{-1/4}$, where A is the surface area available for radiation. Consequently, we would expect

$$\frac{T_3}{T_1} \sim \left(\frac{A_1}{A_3}\right)^{1/4} \quad (4.7)$$

where

$$A_1 = 2 h w \quad (4.8)$$

$$A_3 = 2(\ell_a w + \ell_a h + hw) \quad (4.9)$$

and where T_1 and T_3 denote the mean temperatures in the one- and three-dimensional cases, respectively. For the RM data, we have $(A_1/A_3)^{1/4} \sim 1/2$, so one expects a three-dimensional treatment to yield a temperature a factor of two or so smaller than obtained in the one-dimensional case. However, we also have

$$A_2 = 2(hw + \ell_a h) \quad (4.10)$$

and $(A_3/A_2)^{1/4} \sim 1.15$ for the RM case. Therefore, the expected difference in temperature obtained in a two- and three-dimensional treatment is only about 15%. Thus, the results of the two-dimensional calculation are probably a far more accurate representation of the arc's actual properties than are the one-dimensional results and they are, furthermore, probably not too far from results that would be obtained in a three-dimensional treatment. It is of interest to note that for the RM data

$$(A_1/A_2)^{1/4} \sim 0.58 ,$$

(4.11)

whereas the ratio of the mean temperature in the two-dimensional and one-dimensional calculations (37,000 °K and 57,000 °K, respectively) is 0.65. The two numbers are in fairly close agreement.

In the near future a number of calculations will be of interest. It is first of all desirable to consider higher-order terms in the governing equations in order to include the effects of the rotational motion of the arc discussed previously. It is not likely that these effects will produce any major change in the arc's fluid-dynamic properties, but the importance of the effects does need to be assessed. Second, it will be of interest to study the effects of the plasma upon the projectile and rails. These calculations will provide a first step in evaluating the erosive effects of arc. Finally, some future consideration should be given to time-dependent effects. Only through such treatments can we study the formation and early development of the arc and assess the validity of the steady-state assumption. These problems are slated for study in the near future.

NOTE ADDED IN PROOF: Since completion of this work, the Westinghouse rail gun has been completed and fired several times.¹³ In the most successful firing, a 317-g projectile was accelerated to a velocity of 4.2 km/s in a distance of about 5m. The resulting projectile energy is the largest yet achieved by a rail gun, and the experiment represents a remarkable advance in rail-gun technology.

ACKNOWLEDGEMENT

I am indebted to Dr. J.H. Batteh for many helpful suggestions and much useful discussion.

13. "Laboratory Demonstration Electromagnetic Launcher - EMACK," Commissioning Test Results, Westinghouse R&D Center, Pittsburgh, PA.

REFERENCES

1. John D. Powell and Jad H. Batteh, "Plasma Dynamics of the Arc-Driven Rail Gun," Ballistic Research Laboratory Report No. ARBRL-TR-02267, September 1980. See also "Plasma Dynamics of an Arc-Driven, Electromagnetic, Projectile Accelerator," J. Appl. Phys. 52, 2717 (1981). (AD A092345)
2. R.S. Hawke, A.L. Brooks, F.J. Deadrick, J.K. Scudder, C.M. Fowler, R.S. Caird, and D.R. Peterson, "Results of Rail Gun Experiments Powered by Magnetic Flux Compression Generators," IEEE Trans. Magnetics 18, 821 (1982).
3. Y.B. Zel'dovich and Y.P. Raizer, Physics of Shock Waves and High-Temperature Hydrodynamic Phenomena (Academic, New York, 1966), Vol. I, Chap. 3.
4. C.E. Moore, "Atomic Energy Levels," National Bureau of Standards Circ. No. 467, Vol. II, Washington, DC, 1952.
5. See Ref. 3, Chap. 2.
6. Y.P. Raizer, "Simple Method for Computing the Mean Range of Radiation in Ionized Gases at High Temperatures," Sov. Phys. -JETP 37, 769 (1960). See also Ref. 3, Chap. 5.
7. L. Spitzer, Physics of Fully Ionized Gases, (Interscience, New York, 1965), Chap. 5.
8. R.S. Cohen, L. Spitzer, and P. McR. Routly, "The Electrical Conductivity of an Ionized Gas," Phys. Rev. 80, 230 (1950).
9. L. Spitzer and R. Harm, "Transport Phenomena in a Completely Ionized Gas," Phys. Rev. 89, 977 (1953).
10. R. Courant and D. Hilbert, Methods of Mathematical Physics (Interscience, New York, 1953), Vol. I, Chap. V.
11. S.C. Rashleigh and R.A. Marshall, "Electromagnetic Acceleration of Macro-particles to High Velocities," J. Appl. Phys. 49, 2540 (1978).
12. Author's unpublished calculations.
13. "Laboratory Demonstration Electromagnetic Launcher - EMACK," Commissioning Test Results, Westinghouse R&D Center, Pittsburgh, PA.

DISTRIBUTION LIST

<u>No. of Copies</u>	<u>Organization</u>	<u>No. of Copies</u>	<u>Organization</u>
12	Administrator Defense Technical Info Center ATTN: DTIC - DDA Cameron Station Alexandria, VA 22314	1	Commander US Army Materiel Development & Readiness Command ATTN: DRCLDC, Mr. Langworthy 5001 Eisenhower Avenue Alexandria, VA 22333
1	Office Under Secretary of Defense Res & Engr ATTN: Mr. Ray Thorkildsen Room 3D1089, Pentagon Washington, DC 20301	6	Commander US Army Armament Research and Development Command ATTN: DRDAR-TSS (2 cys) DRDAR-LCA, Mr. J.A. Bennett DRDAR-LCA, Dr. T. Gora DRDAR-LCA, Dr. P. Kemmy DRDAR-SCA-W, R. Goldstein Dover, NJ 07801
1	Deputy Under Secretary of Defense Res & Engr Rm. 3E114, Pentagon Washington, DC 20301		
4	Director Defense Advanced Research Pro- jects Agency ATTN: Dr. Joseph Mangano Dr. Gordon P. Sigman Dr. Raymond P. Gogolewski Dr. Harry Fair 1400 Wilson Blvd Arlington, VA 22209	1	Commander US Army Armament Materiel Readiness Command ATTN: DRSAR-LEP-L, Tech Library Rock Island, IL 61299
1	Office of Assistant Secretary of the Army ATTN: RDA, Dr. Joseph Yang Room 2E672, Pentagon Washington, DC 20310	1	Director US Army ARRADCOM Benet Weapons Laboratory ATTN: DRDAR-LCB-TL Watervliet, NY 12189
1	HQDA (DAMA-ARZ-A, Dr. Marvin Lasser) Washington, DC 20310	1	Commander US Army Aviation Research & Development Command ATTN: DRDAV-E 4300 Goodfellow Blvd. St. Louis, MO 63120
1	Commander US Army Materiel Development & Readiness Command ATTN: DRCDMD-ST 5001 Eisenhower Avenue Alexandria, VA 22333	1	Director US Army Air Mobility Research & Development Laboratory Ames Research Center Moffett Field, CA 94035
1	Commander US Army Amrament Research and Development Command ATTN: DRDAR-TDC, Dr. D. Gyrog Dover, NJ 07801	1	Commander US Army Communications Research & Development Command ATTN: DRDCO-P2A-SA Ft. Monmouth, NJ 07703

DISTRIBUTION LIST

<u>No. of Copies</u>	<u>Organization</u>	<u>No. of Copies</u>	<u>Organization</u>
1	Commander US Army Electronics R&D Command Technical Support Activity ATTN: DELSD-L Ft. Monmouth, NJ 07703	4	Commander Naval Surface Weapons Center ATTN: Henry B. Odom, Code F-12 Dr. M. Franklin Rose, Code F-04 P.T. Adams & D.L. Brunson, Code G-35 Dahlgren, VA 22448
2	Commander US Army Missile Command ATTN: DRSMI-R DRSMI-YDL Redstone Arsenal, AL 35898	1	Commander US Naval Research Laboratory ATTN: Dick Ford, Code 4774 Washington, DC 20301
1	Commander US Army Tank Automotive Research & Development Command ATTN: DRDTA-UI Warren, MI 48090	1	HQ AFSC/XRB ATTN: CPT Dennis Kirlin Andrews AF Base, MD 20331
1	Director US Army TRADOC Systems Analysis Activity ATTN: ATAA-SL, Tech Library White Sands Missile Range, NM 88002	2	AFATL/DLDB (Lanny Burdge) (Bill Lucas) Eglin AF Base, FL 32542
2	Commander US Army Research Office ATTN: Dr. Fred Schmiedeshoff Dr. M. Ciftan PO Box 12211 Research Triangle Park, NC 27709	1	AFATL (Richard Walley) Eglin AF Base, FL 32542
2	Commander Naval Air Systems Command ATTN: Dr. R.J. Wasneski, Code 350F John A. Reif, AIR 350B Washington, DC 20360	1	AFWL (Dr. William L. Baker) Kirtland AFB, NM 87117
		1	AFWL/NTYP (John Generosa) Kirtland AFB, NM 87117
		1	AFAPL (Dr. Charles E. Oberly) Wright-Patterson AF Base, OH 45433
		1	AFWAL/POOS-2 (CPT Jerry Clark) Wright-Patterson AF Base, OH 45433
		1	Director Brookhaven National Laboratory ATTN: Dr. James R. Powell Bldg 129 Upton, NY 11973

DISTRIBUTION LIST

<u>No. of</u> <u>Copies</u>	<u>Organization</u>	<u>No. of</u> <u>Copies</u>	<u>Organization</u>
2	Director Los Alamos Scientific Laboratory ATTN: Dr. Clarence M. Fowler, MS970 Dr. Denis R. Peterson, MS985 Los Alamos, NM 87544	1	Westinghouse Research & Development Laboratory ATTN: Dr. Ian R. McNab 1310 Beulah RD Pittsburgh, PA 15253
3	NASA-LeRC MS 501-7 ATTN: Bill Kerslake Frank Terdan Mike Brasher 2100 Brook Park RD Cleveland, OH 44135	2	Massachusetts Institute of Technology Francis Bitter National Magnet Laboratory ATTN: Dr. Henry H. Kolm, Mr. Peter Mongau NW-14-3102 170 Albany Street Cambridge, MA 02139
1	International Applied Physics ATTN: Dr. John P. Barber 2400 Glenheath Drive Kettering, OH 45400	2	University of Florida ATTN: Prof. K. T. Millsaps Prof. B. M. Leadon Gainesville, FL 32601
1	JAYCOR ATTN: Dr. Derek Tidman 205 S. Whiting Street Alexandria, VA 22304	2	University of Texas Center of Electromechanics ATTN: Dr. Richard A. Marshall Mr. William F. Weldon 167 Taylor Hall Austin, TX 78712
2	R&D Associates ATTN: Mr. Ronald Cunningham Dr. Peter Turchi PO Box 9695 Marina Del Rey, CA 90291	<u>Aberdeen Proving Ground</u> Dir, USAMSAA ATTN: DRXSY-D DRXSY-MP, H. Cohen Cdr, USATECOM ATTN: DRSTE-TO-F Dir, USACSL, Bldg E3516, EA ATTN: DRDAR-CLB-PA	
1	Science Applications, Inc. ATTN: Dr. Jad H. Batteh 6600 Powers Ferry RD Suite 220 Atlanta, GA 30339		
1	Science Applications, Inc. Corporate Headquarters ATTN: Dr. Frank Chilton 1200 Prospect Street La Jolla, CA 92038		